



## SHOCK SYNTHESIS OF SILICIDES—II. THERMODYNAMICS AND KINETICS

M. A. MEYERS, LI-HSING YU and K. S. VECCHIO

Department of Applied Mechanics and Engineering Sciences, University of California, San Diego,  
La Jolla, CA 92093-0411, U.S.A.

(Received 16 September 1992; in revised form 23 July 1993)

**Abstract**—A thermodynamic and kinetic analysis of shock-induced reactions in the (Nb or Mo)–Si systems provides a framework for the extraordinarily high reaction rates and a quantitative interpretation of the experimental results obtained in Part I. The thermodynamic analysis is conducted by adding the heat of reaction to the shock energy; increases in shock pressure, temperature, and velocity are predicted. At the particle level, melting at the silicon–metal interface is found to be a necessary condition for the initiation of reaction; heat conduction calculations enable the prediction of a critical molten (Si) region size for which the heat generated through the reaction exceeds the heat lost to the unreacted regions. The calculation of melt fraction (of Si) as a function of shock energy coupled with critical melt pool sizes enables the determination of a minimum shock energy for the initiation of shock-induced reaction. At the local level, the reaction kinetics can be rationalized through the production of a liquid-phase reaction product (NbSi<sub>2</sub>), the formation of spherical nodules (~2 μm diameter) of this product through interfacial tension and their subsequent solidification (in times of 1–5 ns). The heat generated by the reaction is sufficient to melt niobium along the interface which facilitates both the expulsion of the NbSi<sub>2</sub> nodules into the liquid Si, and the generation of fresh Nb interface for further reaction. In addition, the dissolved Nb enriches the surrounding Si liquid, promoting more NbSi<sub>2</sub> reaction and formation.

### 1. INTRODUCTION

Shock-wave propagation through materials generates significant structural changes; these effects have been the object of extensive studies, that were initiated with the Manhattan project in the early 1940's and continue to this day. Analytical investigations coupled with experimental studies have yielded mechanisms rationalizing the production of dislocations and point defects due to shock-wave passage through solid materials. The first mechanism was proposed by Smith [1], followed by Hornbogen [2] and later modified by Meyers [3] and Weertman [4]. This work is reviewed by Mogilevski [5], who also applied molecular dynamics to explain the generation of defects at the shock front [6]. Weak shock-wave effects have been modeled by Weertman and Follansbee [7, 8]. The effects of shock-wave passage through porous (powder) materials are considerably more complex, because intense and non-uniform plastic deformation is coupled with the shock-wave effects. Thus, the particle interiors experience primarily the effects of shock waves, while the surfaces undergo intense plastic deformation which can result in melting. This localized melting leads to the bonding of the powder, and this gave rise to the research field of shock-wave compaction. A theoretical framework predicting a minimum shock energy and shock pulse duration to create and solidify an interparticle melting layer has been developed by Gourdin [9] and Schwarz *et al.* [10]. This framework has recently been

extended by Potter and Ahrens [11] to ultrahard materials incorporating material strength effects through a Carroll–Holt model. When potentially reactive powder mixtures are used, the shock pulse may trigger these reactions and synthesize new materials. The energy of reaction has to be incorporated into the computations, and efforts by Horie and Kipp [12], Boslough [13], and Yu and Meyers [14] are noteworthy. Recently, Krueger *et al.* [15] and Krueger and Vreeland [16] proposed models that address, in a predictive manner, shock-induced reactions, with the postulation of a threshold energy (provided by the shock wave) for the initiation of reaction.

In this paper, a rational and quantitative analysis is provided for the results reported by Vecchio *et al.* [17], consistent with the threshold energy concept proposed by Krueger and Vreeland [16].

The introduction of exothermic reactions in concurrence with the physical processes under shock compression of porous materials requires special analyses, at the following levels:

- (i) continuum—thermodynamic;
- (ii) local—particle level;
- (iii) local—sub-particle (interface) level.

It will be shown that the extraordinarily high reaction rates encountered under shock conditions can be rationalized and quantified. The experimentally obtained regions where shock-induced reactions

occur are compared with computational predictions in Section 2. An analytical framework that enables a mechanistic understanding of shock synthesis of silicides will be developed in Section 3–5. Through this framework it will be possible to develop quantitative expressions that predict the major effects of shock synthesis.

## 2. COMPUTED SHOCK PRESSURES AND ENERGIES

In order to rationalize the experimental results of the companion paper (Part I) [17], computed predictions of shock pressures and energies within the capsules are important. The contours of partially and fully reacted regions of Fig. 2 of Part I [17] can be correlated to the pressure and energy levels experienced by the powders within the capsules. A strictly one-dimensional strain computation using the equation of state for the Nb–Si mixture developed according to the method described in Section 2 is shown in Fig. 1. These plots were obtained in a simple hydrodynamic code MYIDL, developed by Yoshida [18]. The first pressure pulse, which carries

most of the energy and travels through the porous powder, compacting it, has pressures of  $\sim 7$  and 15 GPa, for the 1.2 and 1.9 km/s impact velocities (these are the impact velocities used in [17]). A second, higher amplitude pulse is initiated at the back surface of the capsule ( $\sim 15$  and 30 GPa, respectively) and travels through the compacted/material. The tri-dimensional effects introduced by the finite lateral dimensions of the capsule are very significant and produce large deviations of pressure and temperature from the values of Fig. 1. The pressure and energy contours predicted using an advanced, two-dimensional CSQ code by Norwood and Graham [19] are shown in Fig. 2. These simulations were conducted using rutile at  $\sim 60\%$  theoretical density as a model material. The pressure levels are at a time of  $1.95 \mu\text{s}$  after the shock wave enters the capsule, and the energy levels are at a time of  $5 \mu\text{s}$  after the shock wave enters the capsule. A spike is seen at the center, along the axis of the disk. This central pressure/energy spike is due to the convergence of the shock from the sides (the shock wave travels faster in the capsule than in the powder, creating a “pincer” action). The energy was obtained from Norwood and Graham’s [19] bulk temperature contours by proper

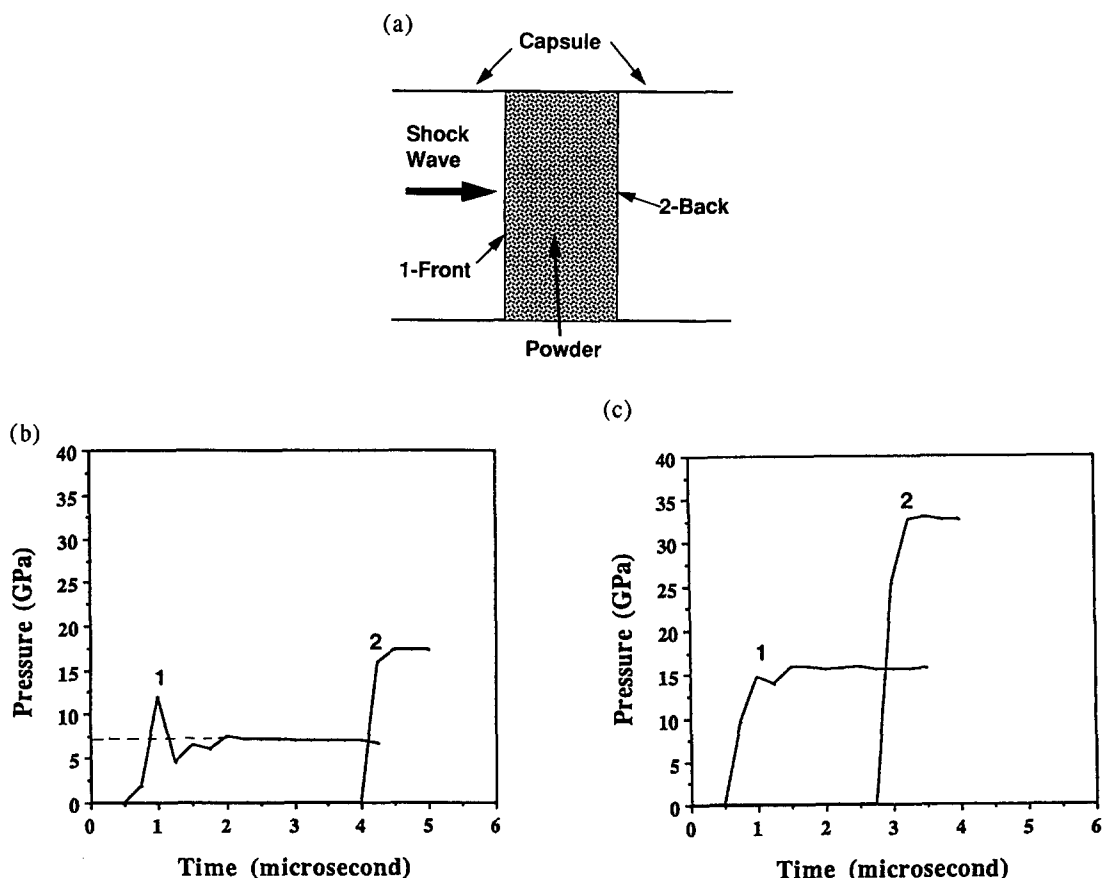


Fig. 1. One dimensional computed pressure as a function of time at front (1) and rear (2) surfaces of the shock capsule; pressure at the front represents amplitude of the first wave, whereas pressure at the back represents amplitude of the reflected pulse (a) computational configuration, (b) profiles for 1.2 km/s impact, and (c) profiles for 1.9 km/s impact.

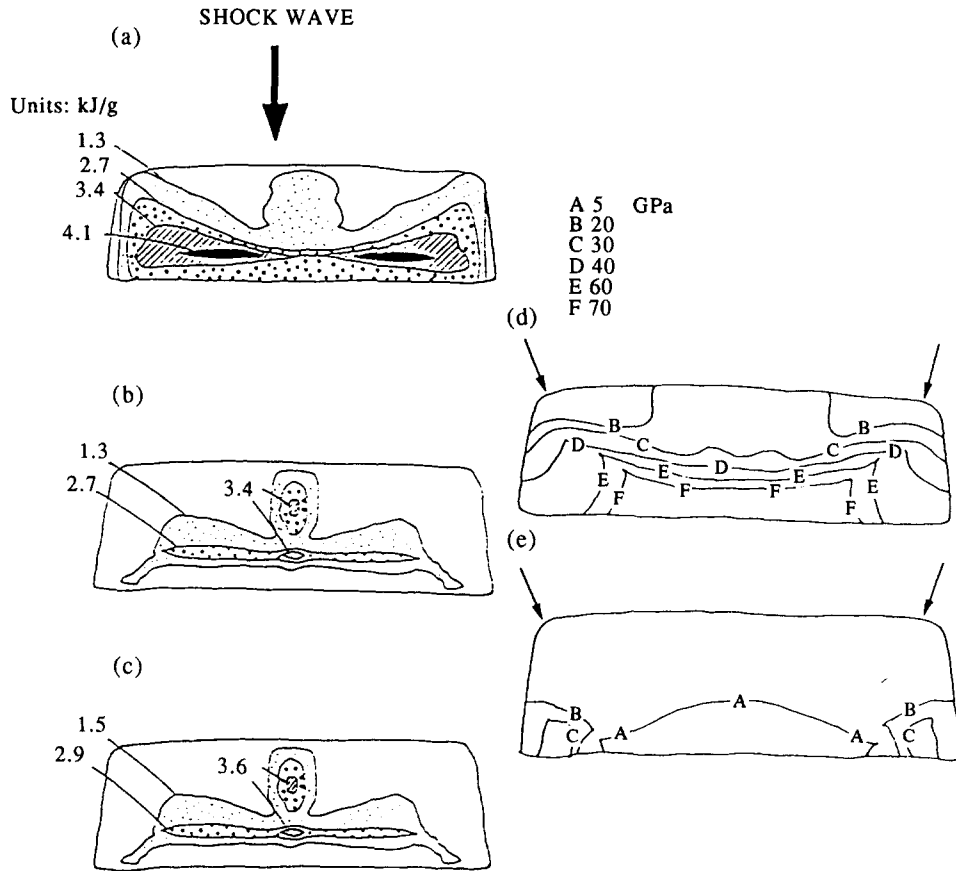


Fig. 2. The summaries of energy contours at a time of  $5 \mu\text{s}$  after shock wave enters capsule for impact velocities: (a) 1.9 km/s at room temperature, (b) 1.3 km/s at room temperature, (c) 1.3 km/s at  $500^\circ\text{C}$ , and pressure contours at a time of  $1.95 \mu\text{s}$  after shock wave enters capsule for impact velocities of (d) 1.9 km/s, and (e) 1.3 km/s.

conversion, using a heat capacity that is the mass average

$$E = \int_{T_0}^T C_v dT. \quad (2)$$

For the  $500^\circ\text{C}$  experiment, the thermal energy of the specimen prior to shocking was added to the shock energy:  $E_{\text{th}} = C_v \Delta T = 220 \text{ J/g}$ . Throughout this paper we will use  $C_p$  and  $C_v$  interchangeably since the volume changes are not appreciable. Thus, the values of the energies are increased by this amount on the curves for the  $500^\circ\text{C}$  experiment; this is a relatively minor change in the level. Figure 2 shows that the top of the capsule undergoes pressures of  $\sim 7$  and  $15 \text{ GPa}$ , for the 1.3 and 1.9 km/s impact velocities, respectively. This is consistent with the one-dimensional computations. However, the pressure and energy levels at other regions are considerably higher, due to the three-dimensional effects. Although a quantitative assessment is not possible, the following observations can be made:

- (a) The partially and fully reacted regions follow more closely the energy contours than the pressure contours. The pressure, at

times earlier than shown in Fig. 2(d,e) reaches very high values at the upper edges of the capsule (marked by arrows), where no reaction was seen to occur. The fully-reacted region is concentrated on the bottom/central portions of the capsule, corresponding to the maximum energies.

- (b) By comparing Fig. 3 of Part I [17] with Fig. 2, it can be seen that a threshold energy of  $600\text{--}800 \text{ J/g}$  is necessary to initiate the reaction for the room temperature experiments in the Nb–Si system. For the  $500^\circ\text{C}$  experiment, this energy seems to be somewhat lower. This threshold energy concept was proposed by Krueger *et al.* [15, 16].

A possible complicating factor not considered in the above comparison between observed and computed reaction profiles is the possibility that reactions can continue after the passage of the shock pulse. The reaction, initiated during the passage of the shock pulse, can continue to completion. This complicates the interpretation of recovery specimens, and has not been addressed quantitatively in the present or past studies.

### 3. THERMODYNAMICS OF SHOCK SYNTHESIS OF SILICIDES

In this section, it will be seen how the threshold energy can be correlated to the state of the sample. The thermodynamics of shock-wave passage through porous materials has traditionally been treated by using the Mie–Grüneisen equation of state (EOS) for a constant volume [20, 21]. Krueger *et al.* [15] developed a theory for the propagation of shock waves through powder mixtures. The treatment used here will be the simple Mie–Grüneisen approach, since accuracy in the equation of state is not essential to the development. The “Mixture” program developed by Yoshida [22] was used in the computation of the equation of state; it is based on the simple mixing of the constituents in the isothermal compression curve, as proposed by McQueen and Marsh [21].

First, the equations of state for the porous Nb–Si and Mo–Si powder mixtures will be calculated under shock compression, assuming that they are inert (no reaction). Secondly, the reaction energy will be added to them. Thirdly, the melting of the components as a function of shock energy will be established.

#### 3.1. Equation of state for porous mixtures

Two components, A and B (Nb and Si or Mo and Si) are considered, and the mass fractions are  $m_A$  and  $m_B$ . The specific volume,  $V$ , internal energy,  $E$ , and heat capacity,  $C_v$ , of the mixture is taken as

$$\begin{aligned} V &= m_A V_A + m_B V_B \\ E &= m_A E_A + m_B E_B \\ C_v &= m_A C_{vA} + m_B C_{vB}. \end{aligned} \quad (3)$$

Similarly, the Mie–Grüneisen parameter (at ambient pressure),  $\gamma_0$ , of the mixture is obtained from the mass average

$$\frac{V_0}{\gamma_0} = m_A \frac{V_{A0}}{\gamma_{A0}} + m_B \frac{V_{B0}}{\gamma_{B0}}. \quad (4)$$

The procedure followed in the calculation is to obtain the isothermal compression curve for the mixture from the isothermal compression curves for the components. From the isothermal states ( $E_T, P_T, V_T$ ) one obtains the Hugoniot states ( $E_H, P_H, V_H$ ) for the mixture by applying the Mie–Grüneisen equation, which relates one state to the other state by the equation

$$E_H - E_T = \frac{\gamma}{V_{H,T}} (P_H - P_T). \quad (5)$$

The conversion from the reference state (isothermal) to the shock state (Hugoniot) is made at a constant volume ( $V_H = V_T$ ), in the Mie–Grüneisen treatment. The shock temperature can be obtained from the reference temperature by

$$E_H - E_T = \int_{T_{298}}^{T_H} C_v dT. \quad (6)$$

The internal energy is defined as (from the conservation of energy equation)

$$E_H - E_0 = \frac{1}{2}(P + P_0)(V_0 - V). \quad (7)$$

For the porous material the initial specific volume of the solid material is simply replaced by the specific volume of the porous material,  $V_{00}(P_0 \sim 0)$

$$E_P - E_{00} = \frac{1}{2}P(V_{00} - V_H). \quad (8)$$

If the porous mixture reacts during the passage of the shock wave, the internal energy equation can be expressed simply as

$$E_{HR} - E_{00} = \frac{1}{2}P(V_{00} - V_{HR}) + mE_R. \quad (9)$$

$m$  is the mass fraction reacted, and  $E_R$  the energy of reaction; this approach was introduced by Boslough [13] and Yu and Meyers [14].

These calculations were conducted for the Nb–Si and Mo–Si powder mixtures, at an initial porosity of 40% ( $V_{00} = 1.4V_0$ ), which corresponds to the initial packing of the powders; the results are shown in Fig. 3. If the reaction takes place at the shock front one expects an increase in pressure and shock velocity; these have been predicted by Boslough [13] and Yu and Meyers [14]. The threshold energy for reaction, assumed to be  $\sim 700$  J/g for Nb–Si and Mo–Si

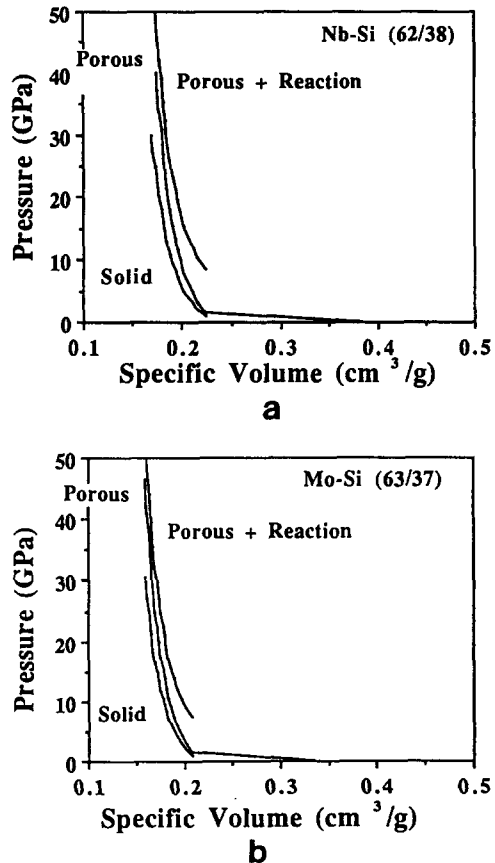


Fig. 3. Equation of state for powder mixtures at 60% of the theoretical density and for mixtures after reaction; (a) Nb–Si; (b) Mo–Si.

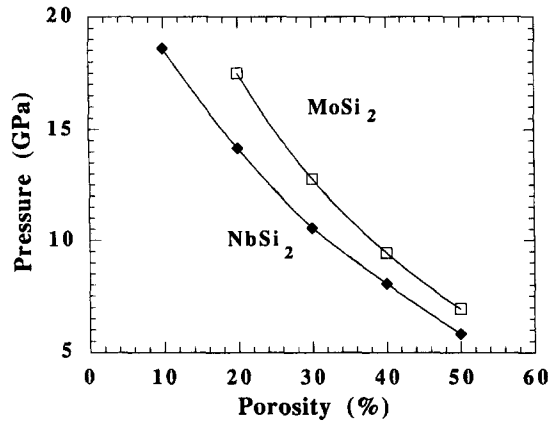


Fig. 4. Predicted (one-dimensional) pressure required to initiate reaction in Nb-Si and Mo-Si systems, as a function of initial porosity.

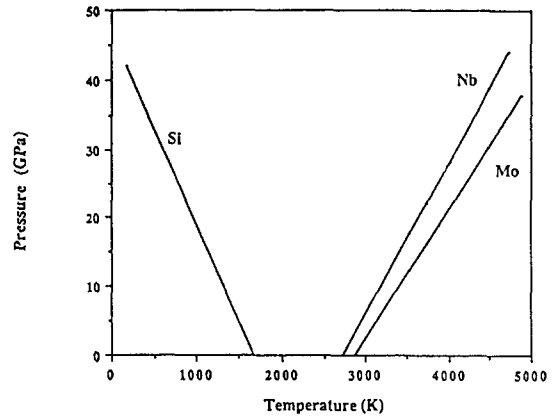


Fig. 5. The effect of shock pressure on the melting points of Nb, Mo and Si.

will be used to calculate a threshold pressure as a function of porosity. This is simply done by solving simultaneously equations (5) and (8). Figure 4 shows the predicted threshold pressures. Higher pressures are required as the porosity of the powder mixture is decreased. This analysis is in agreement with experimental results by Song [23].

### 3.2. Melting as a function of shock energy

The melting of the components is not considered in the EOS graphically expressed in Fig. 3. It is important to determine what the threshold energies correspond to, in physical terms. The shock energy is deposited in the two components. The melting points of the components are determined, as a function of pressure, by the Clapeyron equation

$$\frac{dP}{dT} = \frac{\Delta H}{T_m \Delta V} \quad (10)$$

where  $T_m$  is the melting point,  $\Delta V$  is the volume change in melting, and  $\Delta H$  is the enthalpy of fusion. The effect of pressure is expressed as

$$\begin{aligned} \text{Si: } T &= 1685 + \Delta P \left( -35.7 \frac{\text{K}}{\text{GPa}} \right) \\ \text{Nb: } T &= 2740 + \Delta P \left( 45.7 \frac{\text{K}}{\text{GPa}} \right) \\ \text{Mo: } T &= 2890 + \Delta P \left( 52.93 \frac{\text{K}}{\text{GPa}} \right). \end{aligned} \quad (11)$$

The melting points of the elemental constituents as a function of pressure are plotted in Fig. 5. Silicon has the lowest melting point; additionally, its melting point decreases with pressure because there is a volume decrease associated with its melting. At the one-dimensional pressures of 7 and 15 GPa (Fig. 1), the melting points for silicon are

$$MP_{\text{Si}}^{7\text{GPa}} = 1460 \text{ K}$$

$$MP_{\text{Si}}^{15\text{GPa}} = 1100 \text{ K}.$$

The distribution of the energy deposition between Si and (Mo or Nb) components will establish the energy level at which melting is initiated

$$E = x \left( \int_T^{T_{m1}} C_p dT + \lambda L_f \right)_{\text{Si}} + (1-x) \left( \int_T^{T_{m2}} C_p dT \right)_{\text{Nb}}. \quad (12)$$

$T_{m1}$  is the melting point of Si at the energy level  $E$ ,  $L_f$  is the enthalpy of fusion,  $\lambda$  is the fraction of silicon that is molten,  $x$  is the fraction of energy deposited in Si, and  $(1-x)$  is the fraction of energy deposited in the (Nb, Mo) powder. It is assumed, to a first approximation, that the temperatures in the two components are the same (after Krueger *et al.* [15]). By using the quadratic expressions for the heat

Table 1. Physical and thermodynamic data of Nb-Si, Mo-Si systems

Property	Materials		
	Niobium	Molybdenum	Silicon
Melting temperature (K)	2740	2890	1685
Latent heat of fusion (kJ/mol)	26.79	27.47	39.62
Thermal conductivity (W/cm-K)	0.54	1.38	1.49
Heat capacity ( $C_p$ )	$a = 24.63$	$a = 24.18$	$a = 23.94$
$a + b \times 10^{-3}T + c \times 10^5 T^{-2}$	$b = 3.39$	$b = 1.17$	$b = 2.47$
( $\text{J}^\circ\text{C}^{-1}\text{mol}^{-1}$ )	$c = 9.21$	$c = 0$	$c = 4.14$
Compressive strength (MPa)	200-400	300	90
Main reaction product with Si	NbSi <sub>2</sub>	MoSi <sub>2</sub>	—
Melting temperature of product (K)	2420	2300	—
Heat of reaction to form product (kJ/mol)	138	129.6	—

capacity from Table 1, and equations (11) and (12), one arrives at, for the Nb–Si system

$$\begin{aligned} \frac{1}{2}P(V_{00} - V) = & x[0.295 \times 10^{-3}(1685 - 35.7P)^2 \\ & + 5.72(1685 - 35.7P) + 0.99 \\ & \times 10^5(1685 - 35.7P)^{-1} - 2.06 \times 10^3 \\ & + \lambda 430] + (1 - x)[0.405 \\ & \times 10^{-3}(1685 - 35.7P)^2 \\ & + 5.885(1685 - 35.7P) + 2.2 \\ & \times 10^5(1685 - 35.7P)^{-1} - 2.53 \times 10^3]. \end{aligned} \quad (13)$$

The equation of state from Fig. 4(a) can be expressed as

$$V_{00} - V = -\frac{1}{46.04} \ln\left(\frac{P + 0.0029}{0.0029}\right) \quad (\text{in GPa}). \quad (14)$$

By substituting equation (14) into equation (13), one obtains the melting fraction,  $\lambda$ , as a function of shock pressure,  $P$ , or shock energy,  $E$ . The results are plotted in Fig. 6(a) for two values of  $x$ : 1 and 0.38. When  $x = 1$ , the energy is entirely absorbed by Si. For  $x = 0.38$ , it is uniformly distributed among the two phases in proportion to their mass ratios. Melting of Si starts at an energy of  $\sim 400$  J/g for  $x = 1$  and  $\sim 600$  J/g for  $x = 0.38$ . Melting of Si is complete ( $\lambda = 1$ ) for

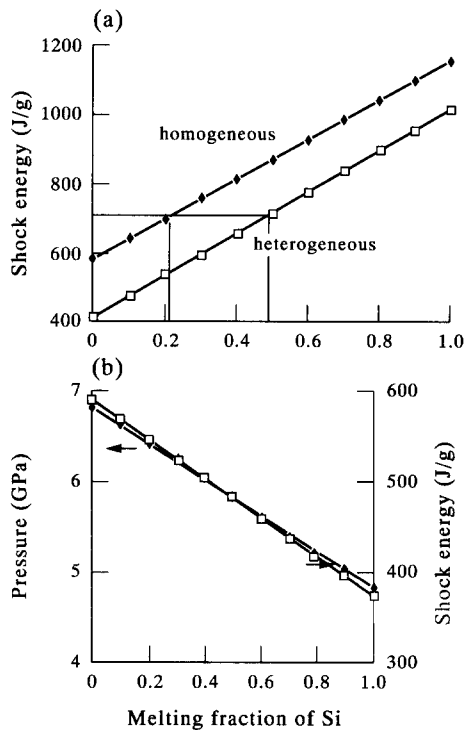


Fig. 6. (a) Melting fraction of Si as a function of shock energy for homogeneous (equally, in Nb and Si) and heterogeneous energy distribution (completely into Si), and (b) melting fraction when energy of reaction is added to shock energy.

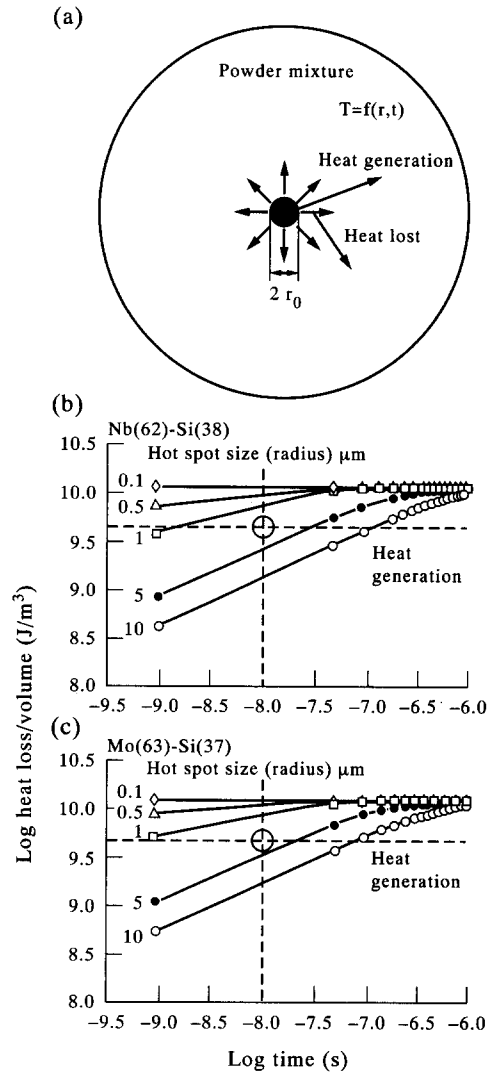


Fig. 7. (a) Molten region with radius  $r_0$  at  $t_0$ ; heat is conducted to the environment, in which the temperature is function of position and time. Calculated heat losses from "hot spots" for different hot spot radii  $r_0$  (0.1, 0.5, 1, 5 and 10  $\mu\text{m}$ ) and heat generation (instantaneous) from shock synthesis of (b) Nb–Si and (c) Mo–Si powder mixtures; heat generation time is  $10^{-8}$  s.

$\sim 1000$  J/g ( $x = 1$ ) and  $\sim 1150$  J/g ( $x = 0.38$ ). The threshold energy level of 700 J/g corresponds to a melting fraction, of Si,  $\lambda$ , between 0.2 and 0.5. This analysis is in accord with the experimental results of Section 2, which indicate that melting of Si is a precondition for reaction. By considering that the molten silicon reacts integrally, and by computing the energy of reaction, the plot of Fig. 6(b) is obtained (for  $x = 0.38$ ). It shows the energy required to propagate the reaction is lower than the energy required to initiate it, and therefore the reaction tends to be self-sustaining.

There is, however, a remaining question: Why is a minimum fraction of molten silicon necessary to initiate the reaction? In order to address this question, a model is proposed below that is based on

the following assumptions, (consistent with the observations of Part 1 [17]):

- (a) melting of silicon is required for the initiation of reaction; and
- (b) a minimum size of reacted materials is required for the propagation of reaction.

Consider an idealized molten pool [Fig. 7(a)] of radius  $2r_0$ , at  $T_{ml}$  and surrounded by material at a temperature  $T_0$ . The reaction of this molten Si with the surrounding solid (Nb or Mo) will generate heat, that is transferred to the surrounding. A general equation that addresses both the heat generation (along the solid-liquid interface, with a surface equal to  $4\pi r_0^2$ ) and heat extraction from this central core, in spherical coordinates, is

$$4\pi r_0^2 \dot{Q} + \rho C_p \frac{\partial T}{\partial t} = k \left( \frac{\partial^2 T}{\partial r^2} + \frac{2}{r} \frac{\partial T}{\partial r} \right) \quad (15)$$

$$\dot{Q} = H_f e^{-\Delta H/RT} H(T - T_{ml}) \quad (16)$$

where  $\rho$  is the density,  $k$  is the thermal conductivity,  $\dot{Q}$  is the heat generation rate,  $H_f$  is the enthalpy of reaction,  $\Delta H$  the activation energy for reaction,  $H(T - T_{ml})$  is a Heaviside function (reaction rate = 0 at  $T < T_{ml}$ , where  $T_{ml}$  is the melting point at the shock pressure). Equation (16) has an implicit assumption: that the reaction stops when the temperature is below the melting point of silicon.

Rideal and Robertson [24] proposed a simpler formalism for the detonation of explosives. They assumed that the heat was instantaneously generated at a hot spot. They calculated the heat extracted from the reacted region as a function of time by using equation (17) (this is the Fourier equation in spherical coordinates)

$$\frac{\rho C_p \partial T}{k \partial t} = \frac{\partial^2 T}{\partial r^2} + \frac{2}{r} \frac{\partial T}{\partial r}. \quad (17)$$

The heat gained by the environment is equal to the heat lost by the hot spot. At a time  $t$ , the heat gained by a spherical shell of radius  $r$  ( $r > r_0$ ) and thickness  $dr$  is

$$dQ = (4\pi r^2 dr) \rho C_p T. \quad (18)$$

By integrating from  $r_0$  to infinity, one obtains the total heat gained by the surrounding (or lost by the hot spot)

$$Q = \int_{r_0}^{\infty} 4\pi r^2 \rho C_p T dr. \quad (19)$$

Figure 7 shows the heat generated and heat lost to environment as a function of time for different "hot spots" sizes; calculations were made for the Nb-Si [Fig. 7(b)] and Mo-Si [Fig. 7(c)] systems. The curves for different hot spot sizes converge to the total value of the heat contained in the hot spot for times on the order 1 ms. Hot spot radii of 0.1, 0.5, 1, 5 and 10  $\mu\text{m}$

were considered. As the hot spot size increases, the time required for the heat to be extracted increases. The heat generated is plotted as a horizontal (dashed) line for the three cases. The heat is actually not instantaneously generated, but over a period that can be approximated as the transit time of the shock wave over a particle. An approximate shock-wave velocity can be obtained from Fig. 1; the capsule thickness is 10 mm, yielding a shock velocity of  $\sim 3 \text{ mm}/\mu\text{s}$ . For a particle diameter of 40  $\mu\text{m}$ , a shock transit time of  $\sim 10^{-8} \text{ s}$  is obtained. The circles on Fig. 7(b,c) correspond to the critical "hot spot" radii for the two materials. These critical "hot spot" sizes for reaction to be initiated are equal to 3 and 4  $\mu\text{m}$  for Nb-Si and Mo-Si systems, respectively. These predictions are in agreement with our experimental results. The critical sizes of these "hot spots" are consistent with the thermodynamic predictions.

#### 4. MODELING SHOCK-INDUCED REACTIONS AT THE PARTICLE LEVEL

An attempt to rationalize the acceleration of reaction kinetics observed in shock compression can be made by analyzing the various terms of an Arrhenius equation, in which both forward and reverse reaction terms are considered. Figure 8 shows the activation barrier necessary to be overcome to react A and B to produce  $A_x B_y$ .  $\Delta G$  is the difference in free energy between products and reactants, while  $\Delta Q$  is the activation energy (enthalpy) for the reaction. Under shock compression, the equation that expresses the rate of reaction has to be modified to incorporate various effects. Figure 8(a) shows three principal effects:

(a) The reactants are in a highly excited state due to the shock passage. High defect densities characterize this state. Panin *et al.* [25] have proposed that under these conditions the material is in a more energetic state.

(b) The activation energy for reaction is decreased because of a "reaction strain" term. If the product (e.g. NbSi<sub>2</sub>) has a lower specific volume than the reactants (Nb and Si), there is an energetic gain with the process, due to local reduction in strain energy. Figure 8(b) shows this effect schematically. Product  $A_x B_y$  occupies a smaller volume than reactants A and B. By a hypothetical procedure devised by Eshelby [26], it is possible to estimate this energy. For purely dilatational strains, Eshelby's equation simplifies itself to

$$E = \frac{1}{2} P \epsilon_v V \quad (20)$$

where  $V$  is the volume transformed,  $\epsilon_v$  the volumetric strain associated with the reaction, and  $P$  is the applied pressure.

(c) The effect of pressure on the thermodynamic equilibrium of the phases. The free energy difference



between products and compounds,  $\Delta G$ , is dependent on the superimposed pressure.

Thus, the Arrhenius rate equation, under shock compression processing (that incorporates both forward and reverse reactions) can be expressed as

$$r = A \exp \frac{-(\Delta Q - \Delta Q_s)}{RT} \left[ 1 - \exp \frac{-(\Delta G + \Delta G_s)}{RT} \right] \quad (21)$$

The terms  $\Delta Q$  and  $\Delta G$  are the activation energy for the reaction and the free energy difference between reactants and products, respectively. The terms  $\Delta Q_s$  and  $\Delta G_s$  results from shock modification, as schematically indicated in Fig. 8(a).  $A$  is a pre-exponential factor related to the attempt frequency. Normalized reaction rates are calculated in the absence and presence of shock compression, for the reaction



The reaction strain (or volumetric contraction) accompanying the conversion of the Nb and Si to  $\text{NbSi}_2$  is 0.29; this corresponds to a reaction strain of 0.11. Considering an applied stress of 14 GPa, one obtains an energy of 178 J/g. The defect energy can be estimated from a dislocation density generated by shock. Assuming a dislocation density of  $5 \times 10^{10}/\text{cm}^2$  (typical of materials shocked to high pressures), one obtains an energy of 9 J/g. This yields:  $\Delta Q_s = 187$  J/g. The free energy of reaction can be taken as  $\Delta G = 926$  J/g. The change in free energy with pressure can be obtained directly from the Clapeyron equation [equation (10)]. It was found to be:  $\Delta G_s = 2477$  J/g.

The activation energy for the formation of  $\text{MoSi}_2$  from elemental Mo and Si has been calculated by Kumar *et al.* [27] and found to be equal to 99.7 kJ/mol. Since the activation energy is not known exactly, a range of values from 100 to 400 kJ/mol was used in the calculations. The pre-exponential factor,  $A$ , is not known and only the ratios  $r/A$  were calculated. The results are shown in Fig. 9(a) for the forward reaction only, and Fig. 9(b) for both forward and reverse reactions. Although shock compression enhances the rate  $r/A$ , the changes are not dramatic. For the forward reaction only, the increase is  $\sim 10\%$ , while considering both forward and reverse rates, the increase is fourfold. These increases are much inferior to the ones observed between the rates of reaction in quasi-static and shock experiments; in the latter, these rates are compared in Section 3 of the companion paper [17]. The shock-induced reaction rate was found to be  $\sim 10^8$  times higher than the solid state, diffusion governed rate. Thus, unless the pre-exponential factor  $A$  is radically different in the two processes, the Arrhenius rate equation shows that the acceleration of the reaction cannot be ascribed to the shock effects above, and has to be indicative

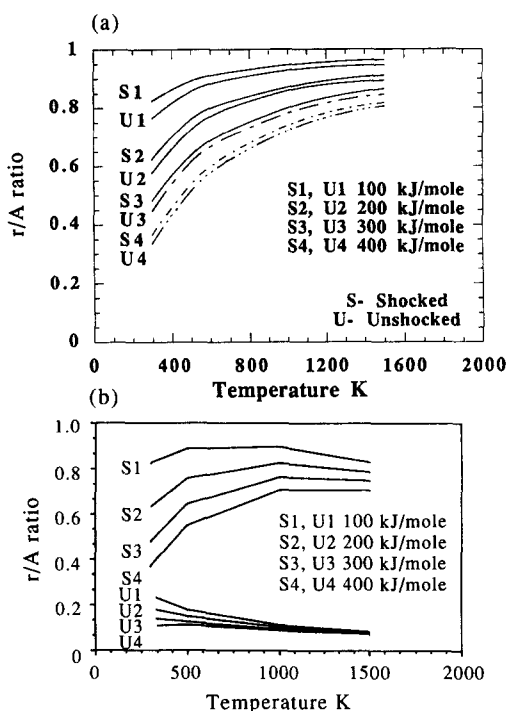


Fig. 9. Reaction rate/pre-exponential parameter ratio as a function of temperature under unshocked and shock conditions; (a) forward reaction only; (b) forward and reverse reactions.

of another mechanism operating. The specific aspects of this new mechanism will be described in Section 5.

It is possible to calculate the overall fraction reacted as a function of time for shock-induced reactions. These global reaction kinetics, as opposed to the local reaction kinetics discussed earlier, are determined by the density of initiation sites, and by the mass reacted per individual event as a function of time. A general formulation will be presented that captures the essential phenomena of the process.

It will be assumed that the initiation sites for reaction will be at particle-particle junctions. The justification for this is that molten pools are observed at particle triple points, in shock consolidation (planar sections). As the particles are accelerated against each other, the molten material is ejected and captured at these regions that are, in a tri-dimensional view, centers of tetrahedra. A tri-dimensional view of a tetrahedral arrangement of spheres is shown in Fig. 10(a). A small sphere in the center indicates the possible initiation site. The initiation sites are the regions where the greatest gaps exist, and where, as a consequence, shock energy is preferentially deposited. The initial density of powders for the silicides was 60% of the theoretical density (TD). This justifies the selection of an idealized body-centered cubic arrangement for the (spherical) particles, with a density of 68% TD. It is assumed that there are  $n$  tetrahedral sites per atom. The mean distance between these sites with respect to a b.c.c. cell, if

the sites are equidistant, is  $d$ . After the consolidation of the unit cell by the shock pressure, the cell size will be reduced from  $2.3 S$  to  $2 S$  ( $S$  is the particle radius). Thus

$$nd^3 = a^3 = 2^3 S^3. \quad (22)$$

There are 24 tetrahedral sites per unit cell, each being shared by two adjacent cells in a b.c.c. arrangement. Thus, one has six initiation sites per particle. For  $n = 6$ , the mean distance between initiation sites is  $1.1 S$ .

If all sites are simultaneously initiated at a time  $\tau_0$  (equal to an incubation time), the fraction transformed at a time  $\tau$  can be estimated by separating the reaction into two stages [Fig. 10(b)]:

- (a) independent reaction events [ $\tau_0 < t < \tau_1$ ; Fig. 10(b) (i, ii)];
- (b) interpenetrating reaction fronts [ $t > \tau_1$ ; Fig. 10(b) (iii, iv)].

The fraction transformed,  $f$ , can be estimated as a function of reaction front advance,  $r$ . If  $n_1$  is the number of initiation sites per unit volume, we have, for  $r_0 < r < d/2$

$$df = n_1 dV = n_1 4\pi r^2 dr. \quad (23)$$

Equation (23) assumes that the reaction is occurring at the surface of a spherical reaction region. Integrating from  $r_0$  to  $r_1$  yields the fraction transformed as

$$f = \frac{4\pi n_1}{3} (r_1^3 - r_0^3). \quad (24)$$

For  $r > d/2$  we have to subtract the overlap volumes of spherical segments  $V_0$  shown in Fig. 10(b, iv). If each initiation site has  $n_2$  nearest neighbors, we have (each overlap volume is shared between two reaction regions)

$$f = n_1 \left[ \frac{4\pi}{3} (r_1^3 - r_0^3) - \frac{n_2}{2} V_0 \right]. \quad (25)$$

But the volume of two juxtaposed spherical caps is

$$V_0 = \frac{2\pi}{3} \left( r - \frac{d}{2} \right)^2 \left( 2r + \frac{d}{2} \right). \quad (26)$$

Thus:

$$f = n_1 \left[ \frac{4\pi}{3} (r_1^3 - r_0^3) - n_2 \frac{\pi}{3} \left( r - \frac{d}{2} \right)^2 \left( 2r + \frac{d}{2} \right) \right]. \quad (27)$$

We can use a Heaviside function,  $H(r - d/2)$ , to generalize the above expression

$$f = \frac{4\pi n_1}{3} \left[ (r_1^3 - r_0^3) - H \left( r - \frac{d}{2} \right) \frac{n_2}{12} \times \left( r - \frac{d}{2} \right)^2 \left( 2r + \frac{d}{2} \right) \right]. \quad (28)$$

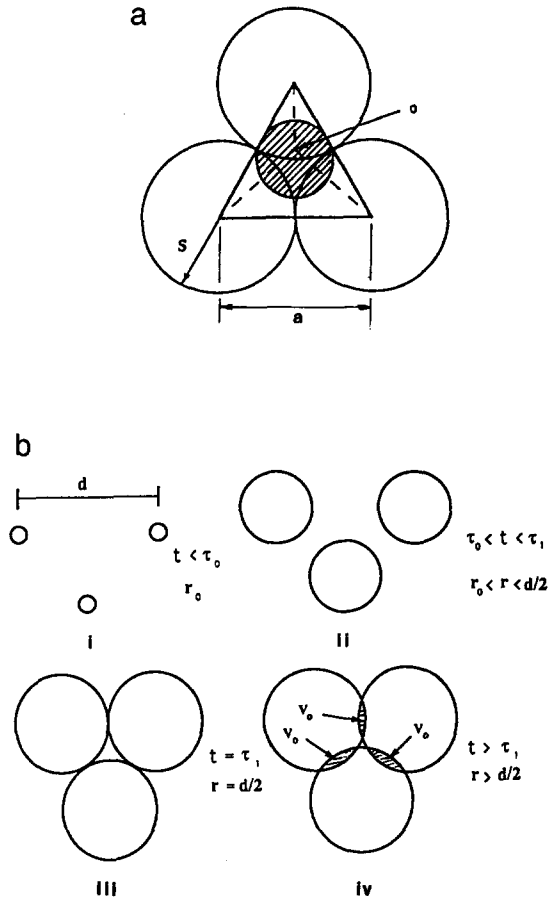


Fig. 10. (a) Tetrahedron formed by spherical particles and center 0. (b) Reacted regions as a function of time; (i) at initiation; (ii) and (iii) during propagation; (iv) during superposition/interaction stage.

The maximum value of  $r_1$  can be estimated as the distance from the center to the vertices of a tetrahedron; or  $0.61 d$ .

The reaction rate,  $\xi$ , is defined as mass reacted per unit area of products/reactants interface. By assuming a constant reaction rate,  $\zeta$ , we can obtain a fraction reacted vs time relationship

$$\zeta = \frac{1}{A} \frac{dm}{dt} = \frac{1}{A} \rho \frac{dV}{dt} = \rho \frac{dr}{dt} \quad (29)$$

$$r - r_0 = \frac{\zeta}{\rho} (t - \tau_0) \quad (30)$$

here again  $\rho$  is the density of the material. Substituting equation (30) into equation (27) (assuming, to a first approximation,  $r_0 = \tau_0 = 0$ ) gives

$$f = \frac{4\pi}{3} n_1 \left( \frac{\zeta}{\rho} \right)^3 \left[ t^3 - \frac{n_2}{12} H(t - \tau_1) \times (t - \tau_1)^2 (2t + \tau_1) \right]. \quad (31)$$

The maximum value of  $t$  is

$$t_{\max} = \frac{\rho}{\zeta} r_{\max} = \frac{0.61\rho d}{\zeta}.$$

The number of initiation sites per unit volume,  $n_1$ , can be expressed as (six initiation sites per particle):  $n_1 = d^{-3} = (1.1S)^{-3}$ . If one considers that each reaction region will overlap with six neighboring regions, then

$$f \cong 3.15 \left( \frac{\zeta}{S\rho} \right)^3 [t^3 - \frac{1}{2}H(t - \tau_1)(t - \tau_1)^2(2t + \tau_1)]. \quad (32)$$

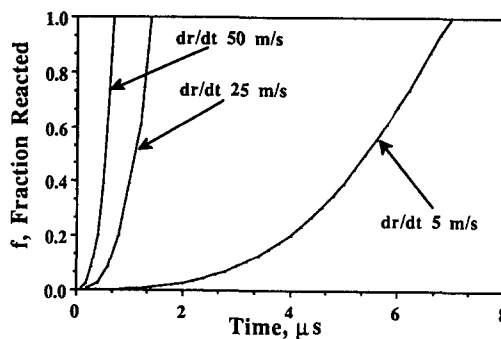
Figure 11 shows plots of the fraction synthesized,  $f$ , as a function of time for different reaction rates,  $\zeta$ , and particle sizes,  $d$ . In Fig. 11(a) the reaction rates are varied for a constant particle size (50  $\mu\text{m}$ ), while in Fig. 11(b) the particle sizes are varied (10, 50, 500  $\mu\text{m}$ ) at a constant reaction rate. These plots are only illustrative since the reaction rates were varied arbitrarily. The reaction rates were assumed consistent with synthesis within the time frames of shock-wave passage. This corresponds  $dr/dt$  values of 5–50 m/s. The particle sizes were varied between 10 and 500  $\mu\text{m}$ . The reaction rates,  $\zeta$ , are obtained from

$$\zeta = \rho \frac{dr}{dt}. \quad (33)$$

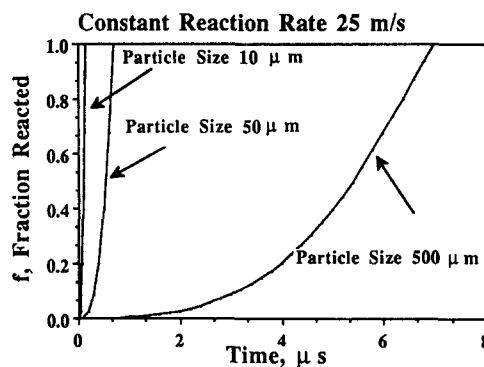
These results show conclusively that the kinetics of synthesis are highly dependent upon both of these parameters. The fraction transformed increases initially with  $t^3$ , and for  $t > \tau_1$ , with  $At^3 - B(t - \tau_1)^2(2t + \tau_1)$ , reaching saturation at  $f = 1$ . Beyond  $\tau_1$  the reaction rate slows down sensibly; this is the sphere overlap region  $0.5d < r < 0.61d$ . Depending on the reaction rate and particle size, the reaction may or may not reach completion during the passage of the shock pulse. These results rationalize the results obtained in Part I [17] (partially and fully reacted regions).

## 5. REACTION MECHANISM

The analysis of the partially reacted regions in the Nb–Si shock experiments revealed the detailed nature of the reaction sequence and mechanisms. There are clear indications that a threshold energy level exists above which the reaction occurs. This is the confirmation of the Krueger–Vreeland [16] suggestion; for the Nb–Si and Mo–Si systems this threshold energy is the level that results in the melting of the pre-established fraction of silicon. The preponderance of small NbSi<sub>2</sub> particles surrounded by silicon, as well as the existence of NbSi<sub>2</sub> particles attached to the niobium particles (Figs 3 and 4 of Part I [17]) are evidence for a reaction mechanism in which the NbSi<sub>2</sub> particles are continuously being generated at the interface and



a



b

Fig. 11. Fraction reacted as a function of time for (a) different reaction rates (constant particle size of 50  $\mu\text{m}$ ) and (b) different particle sizes (constant interface advance rate of 25 m/s).

ejected into the (molten) silicon. Thus, a permanent diffusion barrier (i.e. an interphase layer) that would slow down the reaction process is not formed, and reaction can proceed at a constant rate until the entire niobium or silicon are consumed. The simple calculation below shows that the temperature rise due to the reaction leads to a temperature (locally) higher than the melting point of NbSi<sub>2</sub>. Figure 12 shows the sequence of events envisaged to occur. NbSi<sub>2</sub> will form at a Si–Nb interface, where silicon is molten and niobium solid. Assuming an adiabatic reaction, the temperature is

$$T = T_{\text{MP}}^{\text{Si}} + \frac{\Delta H_r}{C_p}. \quad (34)$$

The enthalpy of reaction of NbSi<sub>2</sub> is (at  $P = 0$ ) equal to 926 J/g. The heat capacity of NbSi<sub>2</sub> was estimated by interpolation between those of Nb and Si on a mass basis ( $m^{\text{Si}}$  and  $m^{\text{Nb}}$  are mass fractions of Si and Nb)

$$C_p = m^{\text{Si}}C_p^{\text{Si}} + m^{\text{Nb}}C_p^{\text{Nb}}. \quad (35)$$

This gives a value of 0.58 J/gK for NbSi<sub>2</sub>. Thus, assuming that the pressure exerted by the shock wave

corresponds to the threshold energy, at 40% porosity, the melting point of silicon is 1400 K (see Figs 4 and 5). This leads to:  $T \approx 3000$  K.

This temperature is considerably higher than the melting point of NbSi<sub>2</sub> (2420 K at  $P = 0$ ). It is therefore likely that the sequence shown in Fig. 12 takes place. The suggestion was made by Glassman [28] that interfacial energy plays an important role in the kinetics of shock synthesis, which led to the development of the following mechanistic model.

Following Fig. 12, the reaction is initiated at (a), along the Nb–Si interface. After reaction has proceeded to a certain extent (c), surface (interfacial) forces become dominant, and the liquid reaction product agglomerates, forming a spherule (e). At this point, reaction kinetics are drastically decreased, because of the reduction of the Nb–Si interfacial area, and solidification of the sphere starts (e). As the sphere solidifies, new nuclei form along the Nb–Si interface (f). They grow, agglomerate into spheres when they reach a critical size, and form neighboring spheres (g). These neighboring regions are constrained and exert forces on the first sphere, expelling it (h) and thus exposing fresh surfaces. This reaction process can continue until the reactants are consumed. As such, no diffusion barrier is formed. The cooling rate of the NbSi<sub>2</sub> spherules can be calculated, and equation (36) shows the effect of time,  $t$ , and distance  $r$ , on temperature,  $T$ , for a spherical particle (spherical coordinates)

$$\frac{\partial T}{\partial t} = \frac{k}{\rho C_p} \left( \frac{\partial^2 T}{\partial r^2} + \frac{2}{r} \frac{\partial T}{\partial r} \right) \quad (36)$$

$$F = \frac{dE}{dy} = \gamma_s \frac{dS}{dy} \quad (37)$$

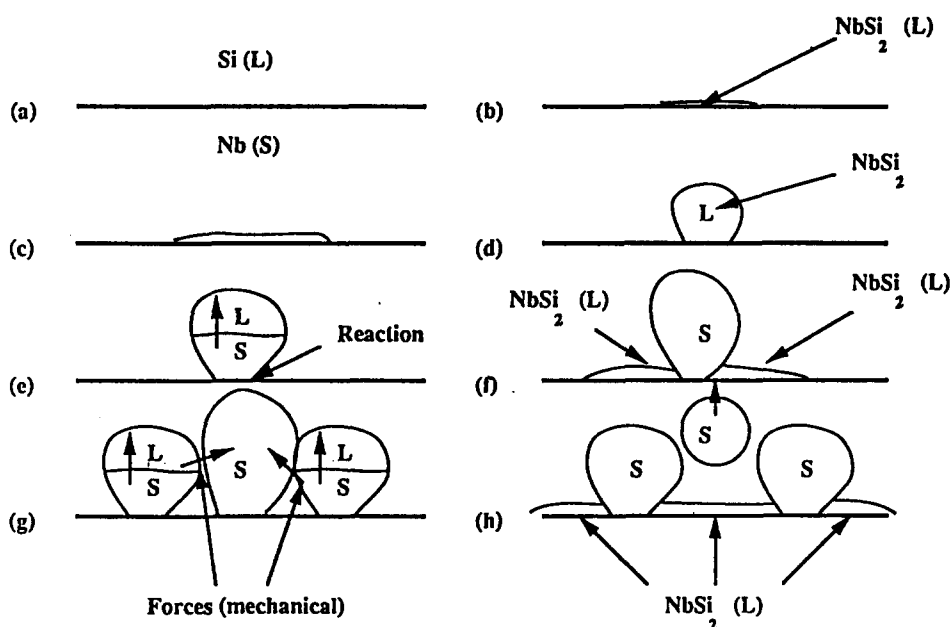


Fig. 12. Sequence of events in the synthesis of NbSi<sub>2</sub> spherules at Nb(solid)–Si(liquid) interface under shock loading; (a–c) nucleation and growth of thin layer; (d) interfacial energy produces spheroidization; (e) solidification and reduced reaction; (f) adjacent reaction regions form in newly exposed interface; (g) spheroidization and solidification of adjacent reaction region; (h) expulsion of spherule.

where  $k$ ,  $\rho$ , and  $C$  are the thermal conductivity, density, and heat capacity, respectively. The initial conditions are

$$T = 3200 \text{ K at } t = 0 \text{ for } r < a, \text{ and}$$

$$T = 1600 \text{ K at } t = 0 \text{ for } r > a,$$

where  $a$  is the radius of the nodule, which can be obtained from measurements in Figs 4, 5, and 10 of part I [17]. An average value of  $2.5 \mu\text{m}$  was taken in the calculations, and values for  $k$ ,  $\rho$ , and  $C$  were averaged from Nb and Si for NbSi<sub>2</sub>. Figure 13 shows the results of the computations using equation (37). The solidification heat is not incorporated into the calculations. Nevertheless, it is clearly seen that solidification can be initiated 2–5 ns after the spherule is formed. Thus, the solidification time is a small fraction ( $\sim 1/1000$ ) of the shock pulse duration time. It is therefore easy to see how successive generations of nodules can be formed, solidified, and ejected from the reaction interface.

The forces that can be exerted by the liquid NbSi<sub>2</sub> on the solid NbSi<sub>2</sub> spherule can be calculated in an approximate manner. These forces are due to the interfacial energy between liquid NbSi<sub>2</sub> and liquid Si as a result of the liquid NbSi<sub>2</sub> attempting to become spherical. A liquid sphere can be flattened into a prolate spheroid by a force  $F$ , as shown in Fig. 14(a). It is possible to calculate this force  $F$ , due exclusively to interfacial energy,  $\gamma_s$ ,

$S$  is the surface area of the spheroid, equal to

$$S = 2\pi b^2 + \frac{2\pi ab}{\epsilon} \sin^{-1} \epsilon. \quad (38)$$

Here  $a$  and  $b$  are the major and minor axes of the spheroid and  $\epsilon$  is the eccentricity, defined as

$$\epsilon = \left(1 - \frac{b^2}{a^2}\right)^{1/2} = \left(1 - \frac{y^2}{x^2}\right)^{1/2}. \quad (39)$$

The volume of the spheroid is constant and equal to  $(4/3)\pi a^2 b$ . By substituting equations (38) and (39) into (37) and eliminating the variable  $a$ , one arrives at

$$F = \gamma_s \left\{ 4\pi y - \frac{3\pi k}{(1 - k^{-2}y^3)^{1/2} y^{1/2}} + \left[ \frac{\pi k y^{-1/2} + 2\pi k^{-1} y^{5/2}}{(1 - k^{-2}y^3)^{3/2}} \right] \sin^{-1}(1 - k^{-2}y^3)^{1/2} \right\} \quad (40)$$

where  $k = r^{1/2}$  and  $r$  is the initial spherule radius.

The interfacial energy for the  $\text{NbSi}_2$  is not known but the surface energy of liquid  $\text{NbSi}_2$  can be estimated from the values of Nb and Si, by interpolation. These values are given by Murr [29]:  $\gamma_s^{\text{Nb}} = 1.9 \text{ J/m}^2$  at  $2473^\circ\text{C}$ ;  $\gamma_s^{\text{Si}} = 0.73 \text{ J/m}^2$ . By interpolation on a mass fraction basis; one obtains:  $\gamma_s^{\text{NbSi}_2} = 1.46 \text{ J/m}^2$ . Close inspection of Table 3.6 from Murr [29] shows that  $\gamma \sim (0.8-1.2) \times 10^{-3} T_m$  for a large number of metals. Since the melting point of  $\text{NbSi}_2$  (2420 K) substan-

tially exceeds that of Si (1685 K) and is close to the melting point of Nb (2740 K), the above estimate is realistic.

Figure 14(b) shows the variation of  $F$  with distance,  $y$ , for a spherical particle with radius equal to  $1 \mu\text{m}$  ( $V = 4/3\pi \mu\text{m}^3$ ). Note that the value of  $F_r$  between  $y = 0.9$  and  $y = 1 \mu\text{m}$  is shown by a dashed line. The formulation breaks down at high values of  $y$ . The force exerted by a prolate spheroid of  $r = 1 \mu\text{m}$  is approximately equal to  $1.5 \times 10^{-5} \gamma_s$ .

From this value it is possible to estimate the total force exerted on a spherule; Fig. 14(c) shows a solid spherule surrounded by liquid prolate spheroids. One can assume that  $n$  spheroids surround one spherule. Thus, the total force is:  $F_T \cong nF$ . The stress exerted by these spherules is approximately equal to

$$\sigma = \frac{nF}{4\pi r_1^2} = \frac{1.5 \times 10^{-5} n \gamma_s}{4\pi r_1^2} \quad (41)$$

where  $r_1$  is the contact area radius, determined by the relative interfacial energies [see Fig. 14(c)]. It is possible to estimate the stresses produced in solid spherules by these surface (interfacial) tensions. An average value of  $2 \times 10^{-5} \sigma_s$  is assumed for  $F$ ;  $r_1$  is assumed to be equal to  $r/2$ ; and one considers that each spherule is surrounded by four prolate spheroids of liquid silicide. Thus,  $\sigma = 28 \text{ MPa}$ .

This stress is of the order of the strength of the silicide. Thus, the stresses can conceivably eject

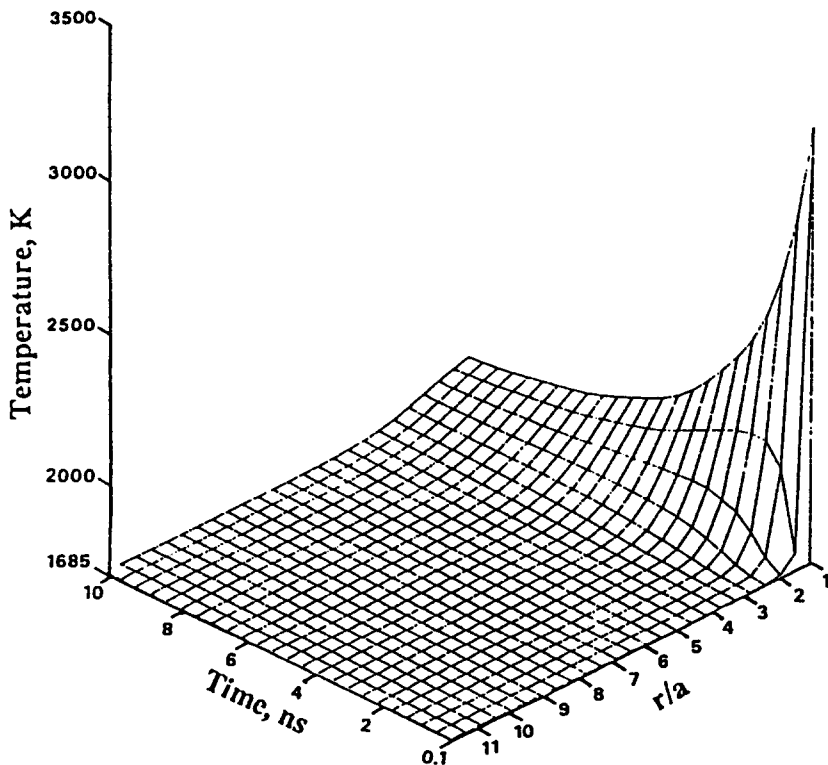


Fig. 13. Heat extraction from spherule with initial temperature of 3200 K while surroundings are at 1600 K.

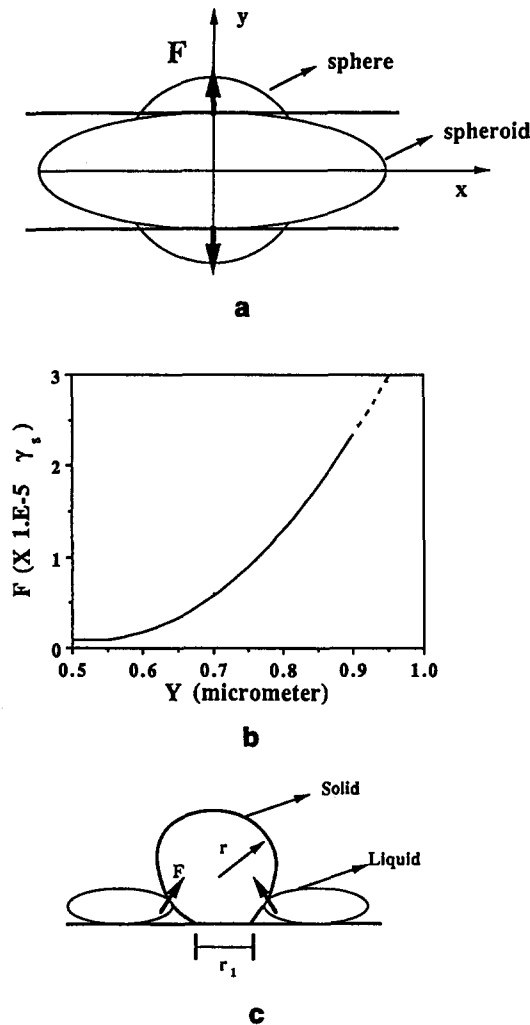


Fig. 14. (a) Prolate spheroid and force  $F$  exerted by surface energy as it is deformed, (b) force,  $F$ , as a function of distance  $y$ , for spherical radius  $r = 1 \mu\text{m}$ , (c) forces,  $F$ , exerted by liquid spheroids on solid spherule.

the solid spherule, and the mechanism proposed is realistic.

Turbulent flow of liquid silicon under shock can also contribute to the detachment of the spherules from the interface; however this mechanism is difficult to quantify. Undoubtedly the drag exerted by the liquid silicon also plays a role, as well as thermal stresses and stress concentrations at the spherule-substrate (Nb) interface. None of these effects have been considered in this analysis; however, they all contribute to more rapid detachment of the  $\text{NbSi}_2$  spherules from the solid Nb interface, thereby making new solid-liquid interface available for subsequent reaction.

## 6. CONCLUSIONS

1. The thermodynamics of shock synthesis was analyzed by considering an equation of state for the porous inert and reactive mixtures. The application

of a threshold energy concept below which no reaction takes place enabled the determination of the critical pressure for reaction as a function of powder density.

2. The fraction of silicon melted as a function of shock energy was calculated and it is found that the threshold energy corresponds to a molten fraction in the range 0.2–0.5 for the Nb–Si system.

3. Heat transfer calculations were conducted in an effort to establish a critical molten region size for which the heat generated by the reaction exceeds the energy dissipated to the environment. Assuming sphericity, these critical radii were found to be equal to 3 and  $4 \mu\text{m}$  for the Nb–Si and Mo–Si systems, respectively. These sizes are qualitatively consistent with observations; the smaller critical shock energy for reaction occurs in the system with the larger heat of reaction and lower thermal conductivity.

4. Reaction kinetics calculations were performed using an Arrhenius equation with forward and reverse rates and modified to incorporate the effects of shock compression. The reaction rate increase that could conceivably be produced by shock compression processing (assuming the same mechanism) is much lower than the one observed in actual experiments, leading to the conclusion that shock compression induces different reaction mechanisms.

5. The global reaction kinetics were calculated by considering a number of initiation sites per unit volume that is a function of powder size. This formulation enables the prediction of the fraction transformed as a function of time and particle size.

6. A reaction mechanism occurring at the (Nb or Mo)–Si interface is proposed. This reaction mechanism involves the dissolution of (Nb or Mo) into molten Si, the reaction producing a molten intermetallic, its spheroidization, solidification, and subsequent expulsion into the liquid silicon melt. In this reaction mechanism a fresh solid (Nb or Mo)–liquid (Si) interface is continuously maintained, enabling a high reaction rate.

*Acknowledgements*—This research was supported by National Science Foundation Grant DMR 8713258 (Materials Processing Initiative), and by McDonnell-Douglas Research Laboratory. We thank the support provided by Dr B. McDonald (NSF) and by Drs C. Whitsett and P. Meschter (MDRL). Discussions with Professor I. Glassman, Princeton University, were extremely helpful in arriving at the mechanism for spherule formation and solidification. The interaction with Dr R. A. Graham, Sandia National Laboratories, through several discussions has provided motivation for this work and contributed significantly to its approach.

## REFERENCES

1. C. S. Smith, *Trans. Metall. Soc. AIME* **212**, 574 (1958).
2. E. Hornbogen, *Acta metall.* **10**, 978 (1962).
3. M. A. Meyers, *Scripta metall.* **12**, 21 (1978).

4. J. Weertman, in *Shock Waves and High-Strain-Rate Phenomena in Metals* (edited by M. A. Meyers and L. E. Murr), p. 469. Plenum Press, New York.
5. M. A. Mogilevski, *Phys. Rep.* **S7**, 359 (1983).
6. M. A. Mogilevski, in *Shock Waves and High-Strain-Rate Phenomena in Metals* (edited by M. A. Meyers and L. E. Murr), p. 531. Plenum Press, New York.
7. J. Weertman and P. S. Follansbee, *Mech. Mater.* **2**, 265 (1983).
8. P. S. Follansbee and J. Weertman, *Mech. Mater.* **1**, 345 (1982).
9. W. Gourdin, *J. appl. Phys.* **55**, 172 (1984).
10. R. B. Schwarz, P. Kasiraj, T. Vreeland Jr and T. J. Ahrens, *Acta metall.* **32**, 1243 (1984).
11. D. K. Potter and T. J. Ahrens, *J. appl. Phys.* **63**, 910 (1988).
12. Y. Horie and M. J. Kipp, *J. appl. Phys.* **63**, 5718 (1988).
13. M. B. Boslough, *J. chem. Phys.* **92**, 1839 (1990).
14. L. H. Yu and M. A. Meyers, *J. Mater. Sci.* **26**, 601 (1991).
15. B. R. Krueger, A. H. Mutz and T. Vreeland Jr, *J. appl. Phys.* **70**, 5362 (1991).
16. B. Krueger and T. Vreeland Jr, in *Shock-Wave and High-Strain-Rate Phenomena in Materials* (edited by M. A. Meyers, L. E. Murr and K. P. Staudhammer), p. 241. Marcel Dekker, New York (1992).
17. K. S. Vecchio, L. H. Yu and M. A. Meyers, *Acta metall. mater.* **42**, 701 (1994).
18. M. Yoshida, Program MY 1DL One-Dimensional Lagrangian Hydrodynamic Code, CETR. New Mexico Institute of Mining and Technology, Socorro, N.M. (1986).
19. F. R. Norwood and R. A. Graham, in *Shock-Wave and High-Strain-Rate Phenomena in Materials* (edited by M. A. Meyers, L. E. Murr and K. P. Staudhammer), p. 989. Marcel Dekker, New York (1992).
20. L. V. Alt'schuler, *Sov. Phys.—USPEKHI* **8**, 2 (1965).
21. R. G. McQueen and S. P. Marsh, in *Behavior of Dense Media Under High Dynamic Pressures*, p. 207. Gordon & Beach, New York (1968).
22. M. Yoshida, Mixture Program, Report. Center for Explosives Technology Research, New Mexico Institute of Mining and Technology, Socorro, N.M. (1986).
23. I. Song, Ph.D. thesis, New Mexico Institute of Mining and Technology, Socorro, N.M. (1991).
24. E. K. Rideal and A. J. B. Robertson, *Proc. R. Soc.* **195**, 135 (1948).
25. V. E. Panin, Yu V. Grinvaev, V. E. Egorushkin, I. L. Buehinder and S. N. Kul'kov, Translation from *Izv. vyssh. Zaved. Fiz.* **1**, 34 (1987).
26. J. D. Eshelby, *Proc. R. Soc.* **9A**, 376 (1957).
27. S. Kumar, J. A. Puszynski and V. Hlavacek, in *Combustion and Plasma Synthesis of High Temperature Materials* (edited by Z. A. Munir and J. B. Holt), Chap. 27, p. 273. VCH Publishers, New York.
28. I. Glassman, Princeton Univ., private communication (1991).
29. L. E. Murr, *Interfacial Phenomena in Metals and Alloys*, p. 131. Addison-Wesley (1975).